Pre-Seeded Optical Scatterers as a Template for Enhancing Order in Inorganic Phototropic Growth

Ethan Simonoff[†,‡], Jonathan R. Thompson[§,‡], Madeline C. Meier[†], Kathleen Kennedy[§], Kathryn R. Hamann[†], Nathan S. Lewis[†,ǁ,*]

[†]Division of Chemistry and Chemical Engineering

[§]Division of Engineering and Applied Sciences

[ǁ]Beckman Institute

[‡]These authors contributed equally

California Institute of Technology

Pasadena, CA 91125

*Corresponding Author: nslewis@caltech.edu

ABSTRACT

Lithographically patterned substrates were used as templates of optical scatterers that seeded the inorganic phototropic growth of Se-Te. Relative to films grown on nominally featureless substrates, films grown on substrates having patterned optical scatterers demonstrated much improved Se-Te pattern fidelities and a narrower distribution of film pattern spatial periods, as quantified by Fourier spectrum analysis. Full-wave electromagnetic modeling and Monte Carlo simulations of Se-Te film growth on substrates with patterned optical scatterers were in good agreement with the patterns observed experimentally. Additional simulations were performed to investigate the limits to pattern period confinement. Simulations revealed that films deposited onto templated substrates can exhibit pattern periods as low as ~80% and as high as ~160% of the pattern period observed for films deposited on non-templated substrates.

INTRODUCTION

We recently described the phenomenon of inorganic phototropic growth, in which the morphology of a growing photoelectrodeposited inorganic material is dynamically determined by the direction, polarization and intensity of an incoherent, spatially uniform, low-intensity illumination source. Inorganic phototropic growth produces nanostructured films with controlled 3-D morphology over macroscopic areas on an optically isotropic electrode substrate using an optically isotropic solution. With polarized optical excitation, an oriented lamellar morphology is formed spontaneously along an arbitrary polarization direction. Phototropic growth of these semiconducting materials occurs via a single-step process that does not utilize chemical or physical templating. Highly anisotropic lamellae resulting from inorganic phototropic growth under uniform, polarized optical excitation conditions have been observed for Se-Te,[1-6] PbSe,[7] and CdSe.[8]

Optical modeling and simulations of the inorganic phototropic growth process have demonstrated that the high-aspect-ratio lamellae formed in phototropically grown films result from a feedback loop initiated by light scattering from an initial collection of nucleated particles that are isotropically distributed on the substrate. The resultant optical scattering however results in localized light absorption in the tips of the emerging lamellae, leading to the observed oriented, directional lamellar growth and morphology. Although the lamellae in phototropically grown films clearly exhibit preferential alignment with the direction of the incident optical polarization, and although increased randomness in the spatial distribution of initial nuclei leads to increased order in the resulting photodeposit, the lamellae obtained to date by inorganic phototropic growth are not perfectly ordered or perfectly aligned spatially over large distances.[5]

Selective and directed growth of materials to yield anisotropy in morphology and function can be enabled through physical or chemical templating. For instance, in a process similar to

nanosphere lithography,[9] a colloidal monolayer of polystyrene beads produces a pattern of contacts that physically block electrolyte at an otherwise conductive working electrode surface, and results in the selective through-pore electrodeposition of zirconia.[10] Chemical functionalization using soft lithography[11] or microcontact printing can also produce a variation in conductivity or reactivity across a substrate.[12] In contrast to physically blocked or chemically modified surfaces, electrodeposition of metals can be directed selectively onto Si microstructures as a result of changes in work function, band conduction, and illumination conditions.[13] Similarly, Ni electrical contacts can be selectively electrodeposited onto Si nanowires, when seeded by Au electrodes.[14]

Pre-seeding of growth substrates can also improve the performance or ensure the desired development of deposited films. Epitaxial growth of GaN requires pre-seeding Al on Si prior to nitriding,[15-16] and epitaxial growth of $PbTiO_3$ on $LaAlO_3$ is markedly improved by pre-seeding with Pb-Ti double alkoxide.[17] Improvements in emission current have been observed when diamond film growth via microwave plasma chemical-vapor deposition (MPCVD) is performed on substrates that are pre-seeded with nanoscale diamond powder.[18] The energy-conversion efficiency of multi-crystalline silicon (mc-Si) solar cells is improved when ingots are grown with mc-Si seeds.[19] The spatial placement of metal catalysts can direct the vapor-liquid-solid (VLS) growth of crystalline (111)-oriented Si microwires by chemical-vapor deposition (CVD) of Si on a crystalline Si substrate.[20] An analogous, solution-based technique to produce TiO_2 nanowires uses pre-seeded ceria nanoparticles dispersed in a solution containing $Ti(SO_4)_2$.[21]

Templating can moreover produce increases in anisotropy in grown materials. In a mild hydrothermal process, pre-seeding substrates with ZnO particles leads to an increase in the aspect ratio of epitaxially grown ZnO nanorods.[22-24] Physical anisotropy in a material can also be obtained by chemical templating methods that produce facet-selective growth or etching, especially in

crystalline material. In contrast to the nanowires normally obtained in the template-assisted electrodeposition of Ni, inclusion of boric acid leads to formation of Ni nanotubes.[25] In the presence of chemical additives such as sodium dodecyl sulfate (SDS) or copper nitrate, electrodeposited cuprous oxide exhibits facet-selective growth during bottom-up synthesis.[26] In a top-down etching procedure, Au microcrystals can be selectively etched in either the (100) or (111) direction with silver tetraoctylammonium bromide (AgToABr) or $Cu(Cl)_2$, respectively.[27] Mass availability,[28-29] pH,[30] growth kinetics,[31] heat flux,[32] local light absorption,[33-34] the applied deposition potential during electrodeposition,[26, 35] and other conditions can also produce anisotropy in developing materials.

Herein we explore the effect of pre-seeded optical scatterers, in the form of a lithographicaly templated substrate, on the inorganic phototropic growth process. The feedback mechanism during inorganic phototropic growth spontaneously produces an ensemble of regularly distributed optical scatterers that in turn produce a focused interference pattern which shapes the near-field light intensity in the growing material. This feedback manifests as the emergent property of inorganic phototropic growth, and results in the observed ordered morphology in phototropically grown inorganic films. If the limited long-range order in the phototropically grown film is a direct consequence of a distribution of scattering distances resulting from spatially distributed nucleates in the initial-phase dark, seed film growth, then pre-positioning of ordered seeds of optical scatterers should yield improved long-range order in phototropically grown films. Moreover, control over the positions of the initial scatterers could yield control of, and new features in, inorganic phototropic growth patterns and morphologies. Hence, control of the initial distribution, density and placement of optical scatterers could bias the phototropic growth process to result in film morphologies and growth patterns that are not accessible by randomly seeded

scatterers. Alternatively, preseeding of scatterers could potentially reduce, or eliminate entirely, long-range order in the resulting films, due to competing effects between the naturally arising emerging interference pattern and the interference pattern produced instead by a spatially incommensurate template of optical scatterers. Templated substrates of scatterers can also provide information on the effective distance of the scattering effect that fundamentally underpins the phototropic growth process. Hence, as part of this work, preseeded scatterers have been lithographically defined and ordered on a length scale commensurate with the dimensions of a single pair of lamellae. Additionally, the characteristics of film growth have been compared to substrates for which the distance between preseeded scatterers is a larger integer multiple of the distance between lamellae that are spontaneously produced by the inorganic phototropic growth process.

EXPERIMENTAL METHODS

Materials and Chemicals SeO_2 (Aldrich, 99.999% trace metals basis), TeO_2 (Aldrich, 99.995% trace metals basis), Buffer HF Improved (BHF) (Transene, Ammonium Hydrogen Difluoride Solution), H_2SO_4 (J.T. Baker, 90-100%), Ga (Alfa Aesar, 6mm diameter pellets, 99.9999% trace metals basis), In (ESPI Metals, shot, 99.9999%), Ti (Kurt J. Lesker, 1/8" Diameter x 1/8" Long, 99.995% Pure), Pt (Kurt J. Lesker, 1/8" Diameter x 1/8" Long, 99.99% Pure), Acetone (BDH, ACS Grade, 99.5% min.), Isopropyl Alcohol (BDH, ACS Grade, 99.5% min. and VWR, 99.5%), poly(methyl methacrylate) (PMMA) (MicroChem 950 PMMA A3), methyl isobutyl ketone (J.T. Baker, >90%), and Ir wire (Alfa Products, 1mm dia., 99.9%) were used as received. H_2O (Barnstead Nanopure Infinity Ultrapure Water System, ρ = 18.3 MΩ-cm) was used throughout.

For working electrodes, n^+-silicon (Addison Engineering Inc., As-doped, ρ = 0.001-0.004 Ω-cm, [111], 525 ± 25 μm thick, SSP) was used. For electrode construction, Loctite 1C Hysol Epoxy Adhesive, Conductive Silver Paint (SPI Supplies), Clear Nail Polish (Sally Hansen "Hard as Nails Xtreme Wear"), tinned Cu wire (AWG 22), and glass tubing (7740 Borosilicate Pyrex, 9mm OD x 1.0mm wall thickness) were used.

Preparation of Pt Substrates Pt-coated n^+-Si substrates used as working electrodes in the deposition of Se-Te were fabricated via electron-beam evaporation of target metals onto n^+-Si wafers. Before being loaded into the vacuum chamber of the electron-beam evaporator, n^+-Si wafers were etched in BHF for a minimum of 20 s to remove native silicon oxides. To make ohmic contact to the n^+-Si, 15 nm Ti was evaporated onto the top (polished) side of the n^+-Si wafers. Without breaking vacuum, 100 nm Pt was then evaporated onto the Ti-coated n^+-Si wafers.

Preparation of Templated Substrates E-beam resist (PMMA) was spin-coated onto Pt substrates at 3000 rpm for 1 min to obtain an ~100 nm thick layer, which was then cured for 5 min at 180 °C. Patterns consisting of 100 nm wide lines with center-to-center distances of 187.5, 242, 375, 484, 726, 750, and 1500 nm were made in AutoCAD and fractured in Layout BEAMER. A Raith Electron Beam Pattern Generator (EBPG) 5000+ was used to write the patterns, with a 5 nA beam and 900 $\mu C\ cm^{-2}$ dose, at 100 kV. After patterning, the resist was developed by immersion for 50 s in a solution of 1:3 (by volume) of methyl isobutyl ketone to isopropyl alcohol. Development was stopped by immersion in isopropyl alcohol, and the substrate was dried under a stream of flowing $N_2(g)$ and cleaved into small (~0.1-0.2 cm^2) chips.

Following patterning via electron-beam lithography, 50 nm of Ti was deposited onto patterned substrates via electron-beam evaporation. Liftoff was performed by sonicating for 30 min in acetone. Following liftoff, an additional 70 nm of Pt was deposited via electron-beam evaporation, to yield the templated substrates.

Fabrication of Working Electrodes The unpolished side of templated and non-templated Pt wafer chips were scratched with prepared Ga-In eutectic (75.5 wt. % gallium, 24.5 wt. % indium) using a carbide-tipped scribe. Electrode mounts were fabricated from tinned Cu wire affixed with inert epoxy to borosilicate glass tubes. Wafer chips were then attached with silver paint to the exposed wire of the electrode mounts. After a minimum of 30 min, the electrodes were sealed and electrically insulated with clear nitrocellulose nail polish.

Fabrication of Iridium Wire Electrodes A piece of Ir wire (~30 mm) was soldered to a segment of tinned Cu wire and placed in a borosilicate glass tube. The soldered contact and glass tube opening were insulated with inert epoxy.

Photoelectrochemical Depositions All electrochemical experiments were performed using a Biologic VMP3 Potentiostat, controlled via EC Lab for Windows. The light intensity was measured using a calibrated Si photodiode (Thorlabs FDS100). A three-port Pyrex glass electrochemical cell with an optical glass window was utilized for all photoelectrochemical depositions.

For electrochemical experiments, a three-electrode configuration was used with an Ir wire counter electrode and a Ag/AgCl (3M NaCl, BASi RE-5B) reference electrode. Working electrodes were Pt and templated substrates. The electrodeposition bath was an aqueous solution of 1.0 M H_2SO_4, 0.020 M SeO_2, and 0.010 M TeO_2. Before deposition, electrodes were rinsed with H_2O. Films were deposited until a charge density of -750 mC cm^{-2} had been passed. The applied deposition potential was -100 mV vs. Ag/AgCl. The light source used during all depositions was a red Thorlabs LED (Thorlabs M625L4). The LED had an intensity weighted average wavelength of 630 nm, a spectral bandwidth of 17 nm, and was powered by an LED driver and power supply (Thorlabs LEDD1B and KPS101). The output from the LED was passed through a linear polarizer (Thorlabs LPVISE200-A) and collected with an aspheric condenser lens (Edmund Optics, Ø = 75 mm, f = 50 mm). A 600 grit diffuser (Thorlabs DG20) was placed in front of the window of the electrochemical cell to produce illumination of uniform intensity incident on the working electrodes. An illumination power density of 50 mW cm^{-2} was used during the photoelectrochemical deposition.

Sample Preparation and Image Acquisition After electrodeposition, a razor blade was used to remove samples from their electrode mounts. An acetone bath was used to remove residual nitrocellulose nail polish and silver paint. Scanning-electron microscopy was performed using an FEI Nova NanoSEM 450 with an accelerating voltage of 5 kV. A through-lens (immersion)

secondary-electron detector was utilized at a working distance of 5 mm. Compositional analysis was performed using an electron dispersive X-ray spectroscopy (EDS) module. Images were either obtained at a magnification of 6250 X or 25 kX. Image resolution was either 4096 or 2048 pixels wide, respectively. Gwyddion (gwyddion.net) was used to perform Fourier analysis on the large-area images (obtained at 6250 X).

Optical Modeling and Growth Simulation The growths of the photoelectrochemically deposited films were simulated with an iterative growth model in which electromagnetic simulations were first used to calculate the local photocarrier-generation rates at the film surface. Then, mass addition was simulated via a Monte Carlo method wherein the local photocarrier-generation rate weighted the local rate of mass addition along the film surface.

Growth simulations began with a semi-infinite planar Pt substrate patterned with 100 nm wide platinum ridges spaced 200 nm, 242.5 nm, 300 nm, 400 nm, 485 nm, 600 nm, and 727.5 nm apart. In the first step, the light-absorption profile under a linearly polarized, plane-wave illumination source was calculated using full-wave finite-difference time-domain (FDTD) simulations ("FDTD Solutions" software package, Lumerical) with periodic boundary conditions along the substrate interface. In the second step, a Monte Carlo simulation was performed in which an amount of mass, equaling that of a 15 nm planar layer covering the simulation area, was added to the upper surface of the structure with a probability F:

$$F(G) = G\prod_{i=1}^{3}\frac{x_i}{r_i} \quad \textbf{(Equation 1)}$$

where G is the spatially dependent photocarrier-generation rate at the deposit/solution interface, x_i is the fraction of ith nearest neighbors occupied in the cubic lattice, and r_i is the distance to the ith nearest neighbor. The multiplicative sum in the definition of this probability (Equation 1) serves to reduce the surface roughness of the film and consequently mimic the experimentally observed

surface roughness. A value of n = 1.33 was used as the refractive index of the growth solution, regardless of wavelength.[36] Simulations of the film morphology utilized the intensity-weighted average wavelengths, λ_{avg}, of the experimental sources. The electric-field vector of the illumination was aligned to the orientation of the templated pattern. A two-dimensional square mesh with a lattice constant of 10 nm was used for the simulations. After the initial Monte Carlo simulation, the absorbance of the new, structured film was then calculated in the same manner as for the initial planar film, and an additional Monte Carlo simulation of mass addition was performed. This process of absorbance calculation and mass addition was repeated for a total of 15 iterations.

RESULTS

1. Characteristics of Phototropically Grown Se-Te Films Formed on Unpatterned Pt-coated n^+-Si Substrates

Figure 1a shows a representative scanning-electron microscope (SEM) image of a phototropically grown Se-Te film deposited potentiostatically onto a Pt substrate. All films (including the film shown in Figure 1a) were deposited under normally incident, vertically polarized light from a narrow-band LED with λ_{avg} = 630 nm at a power density of 50 mW cm^{-2}. The applied deposition potential was -100 mV vs. Ag/AgCl and depositions were performed until a charge density of -750 mC cm^{-2} had been reached. Despite the lack of any optical anisotropy in the substrate or in the solution, the phototropically grown films clearly exhibited a preferential alignment of lamellae along the (arbitrary) direction of the incident optical polarization. The observed average 242 nm period between lamellae is in accord with observations and expectations for inorganic phototropic growth of Se-Te from a deposition solution and growth medium with an index of refraction, n, of ~1.3 (corresponding to the theoretical and observed trend of period = $\lambda/2n$).[1-4]

Figure 1b shows a section of a 2D Fourier transform (2D FT) spectrum of a large-area SEM image of the film shown in Figure 1a. In a 2D FT spectrum, a real-space image is converted to frequency (reciprocal) space. Phase information may be preserved but is not obvious or straightforward to represent, hence spectra in this study were used solely for analysis of the spatial characteristics of the phototropically grown deposit. The features in the 2D FT spectra thus correspond to the frequency of white value in the real-space images. The white value is assumed to be representative of the mass and z-height in the SEM images so the features in the 2D FT spectra consequently represent the arrangement of the film mass in real space. In a 2D FT

spectrum, the distance between the origin (center of the spectrum) and intensity at an arbitrary point is inversely proportional to distance in the real-space image. The vector between the origin and that intensity corresponds to the orientation of the spacing present in the real-space image. Thus, in Figure 1b, features in the 2D FT spectrum correspond to both the orientation and period of the patterns present in Figure 1a. Lorentzian fits to the surface profiles of the primary peaks in 2D FT spectra can be used to assess and quantify the fidelity (straightness) and period (average spacing) of the pattern in the film (see Figure S1 and S2).

2. Characteristics of Spatially Patterned Pt-coated n^+-Si Substrates

Figure 2 shows SEM images of a Pt-coated n^+-Si substrate templated to contain vertically oriented Pt ridges. The material also contains a Ti interlayer that was fabricated via electron-beam lithography and electron-beam evaporation. The ridges were ~ 100 nm tall by 100 nm wide and were deliberately spaced with a pitch of 242 nm (Figure 2a), 484 nm (Figure 2b), or 726 nm (Figure 2c). These spacings between the Pt ridges correspond to 1x, 2x, and 3x the period expected for inorganic phototropic growth of Se-Te lamellae when the growth is stimulated by 630 nm illumination on an isotropic, unpatterned substrate (i.e. Figure 1a). The inset images in Figure 2 are sections of 2D FT spectra of large-area SEM images of the respective films. In contrast to Figure 1b, the features in the 2D FT in Figure 2 are confined vertically, as expected for the more vertically aligned and much straighter features on the templated substrates. Clearly the discontinuity and regular undulation of the lamellar morphology in Figure 1a therefore contribute to substantial broadening of features in the 2D FT displayed in Figure 1b.

3. Characteristics of Phototropically Grown Se-Te Films on Spatially Patterned Pt-coated n^+-Si Substrates

Figure 3 shows SEM images of representative regions of Se-Te films deposited on templated substrates having nominally the same pitches as those in Figure 2. The films shown in Figure 3 were all deposited on one sample that contained several patterned regions as well as unpatterned regions. Thus, all of films shown in Figure 3 were deposited under nominally and locally identical conditions. The film shown in the SEM image in Figure 3d corresponds to an unpatterned region that was optically isolated (spacing $\gg 10\ \lambda$) and physically remote from the patterned regions that are displayed in Figure 3a-c. The 2D FT spectra shown in Figure 3e-h were generated from large-area SEM images of the films in Figure 3a-d, respectively.

The SEM images and 2D FT spectra in Figure 3 illustrate the substantial, obvious increase in pattern fidelity of the phototropically grown Se-Te films that was obtained by use of physically templated substrates. Specifically, the films in Figure 3a and b show little or no defects and display excellent vertical alignment. The high fidelity of these films is also evidenced by the extremely sharp features in the 2D FT spectra shown in Figures 3e and f.

All of the templated phototropically grown films demonstrated improved fidelity compared to the film deposited on non-templated substrates shown in Figure 3d. The 2D FT spectra of the templated films also demonstrated highly defined and localized features compared to the relatively broad peaks observed in Figure 3h. The film in Figure 3c is slightly defective, with a few instances of discontinuity and branching of the lamellar morphology. The degree of defectiveness is also revealed by the broadening and lower definition of features in the 2D FT spectrum in Figure 3g relative to the 2D FT of Figure 3e.

Figure 4 shows overlapping images from Figure 2 and 3, highlighting the relationship between the spacing of phototropically grown Se-Te lamellae and the underlying templated Pt ridges. As expected, the spacing of the Pt templates corresponded precisely to either every lamella

(Figure 4a, 242 nm spacing); every other lamella (Figure 4b, 484 nm spacing); or every two lamellae (Figure 4c, 726 nm spacing).

The results of 2D FT analysis performed on phototropically grown films deposited on templated and non-templated substrates, including those shown in Figure 2 and 3, are given in Figure 5. Figure 5a gives the average measured vertical full width at half maximum (FWHM) for the primary peak in 2D FT spectra of phototropically grown films deposited on templated and non-templated substrates. The vertical FWHM is reported in degrees and was generated by converting the 2D FT spectra from Cartesian to polar coordinates (see Figure S2 and Equation S1). This angular value is a figure-of-merit for the pattern fidelity, in which smaller values correspond to a relatively higher pattern fidelity and straighter lamellae (lower angular spread). The data show that relative to films deposited on substrates with no template (vertical FWHM, θ, of ~30°), the pattern fidelity was greatly improved for phototropically grown films deposited on templates with spacings at 1x (242 nm) or 2x (484 nm) the pattern period, with the resulting 2D FT exhibiting a vertical FWHM of <1°. For phototropically grown films deposited on templates with a spacing of 3x the pattern period (726 nm), the results were less reproducible, but ranged from a similar level of fidelity and order as the obtained for 1x and 2x template spacing (θ = ~1°) to only a marginal improvement relative to films deposited without templates (θ = ~20-25°). Pattern fidelity was also improved in the z-direction, with phototropically grown films demonstrating straight, high-aspect ratio lamellae (Figure S3).

Figure 5a also contains the vertical FWHM values for the template substrates. The templated substrates were lithographically patterned, so the only spatial defects in the pattern were due to errors in the fabrication process. No branching or undulation of the pattern is expected, and consistently the templates consisted solely of multiple and mutually parallel lines. The vertical

FWHM values for the templated substrates were predictably small, corresponding to high pattern fidelities. For substrates with a template spacing of 242 nm or 484 nm, the relatively high pattern fidelities of the template were retained by the phototropically grown films, as demonstrated by the vertical FWHM values in Figure 5a.

Figure 5b presents the average measured period for phototropically grown films deposited on templated or non-templated substrates, respectively. The pattern period was defined from the centroid frequency of the primary peak in the 2D FT spectra. For films on templated substrates, the pattern period was very close to the 242 nm value of the pattern itself. The standard deviations were relatively small, with values of ~0.5 nm for a template spacing of 242 nm or 484 nm and a standard deviation of ~2 nm for a template spacing of 726 nm. In contrast, the pattern period exhibited a relatively larger range of values, with a standard deviation of ~8 nm, for films grown on non-templated substrates. The data thus clearly indicate that the templated substrates confined the spatial period of phototropically grown films to a relatively more precise range of values than observed for phototropically grown films on non-templated substrates. This effect was stronger when templates with smaller spacing were used (i.e. 242 nm vs. 726 nm). This phenomenon is also illustrated by the alignment of the templated substrates and resulting films shown in Figure 4.

4. Modeling and Simulation of Phototropic Growth on Spatially Patterned Substrates

In previous studies we have successfully demonstrated simulated phototropic growth of Se-Te, PbSe, and CdSe using an optically based, two-step, iterative model.[1, 7-8] Additional details for this modeling process are provided in the Experimental Methods section. Figure 6 shows simulations of the initial-, intermediate-, and final-stage phototropic growth of Se-Te on Pt substrates that were templated with Pt ridges spaced at either ~242 nm (Figure 6a-c), ~484 nm (Figure 6d-f), or ~726 nm (Figure 6g-i). In accord with the experimental observations (Figure 3-

5), the simulated growths exhibited improved fidelity and straighter features on template substrates than on unpatterned substrates. Moreover, the most substantial improvements in simulated pattern fidelity occurred when the templates were either in perfect registry with the Se-Te lamellae (i.e. ~242 nm spacing in Figure 3a and 6c) or had a pitch that corresponded to the spacing between every other lamella (i.e. ~484 nm spacing in Figure 3b and 6f). Substantial pattern defects were observed in the simulated growths when the templates were spaced at distances that corresponded to every two lamellae (i.e. ~726 nm spacing in Figure 3c and 6i), although the simulated pattern fidelity was still improved relative to the simulated growth on substrates that were not templated (Figure S4).

A set of phototropic growth simulations was also performed on templated substrates that had spacings that were out of registry with the natural period (~242 nm) (Figure 7). The simulations included templated substrates with 50 nm tall x 100 nm wide Pt ridges with spacings of 200 nm (Figure 7a-c), 300 nm (Figure 7d-f), 400 nm (Figure 7g-i), and 600 nm (Figure 7j-l). All of the periods of the simulated growths on these templated substrates (Figure 7) were substantially different from the natural lamellar period observed and simulated under these optically stimulated growth conditions on a non-templated substrate (~242 nm). Figure 8 gives the measured periods of the templated substrates as well as the periods obtained from analysis of the phototropic growth simulations of Figure 7. The measured periods of the simulated phototropic growths were 199 ± 1, 299 ± 2, 398 ± 3, and 299 ± 2 nm for templates having pitches between Pt lines of 200 nm, 300 nm, 400 nm, and 600 nm, respectively. The results in Figure 8 indicate that the Pt templates confined the optical scattering and enforced a pattern period over a wide range of spacings. For example, for the 200 nm, 300 nm, and 400 nm pitch templates, the period of the simulated final-stage film had essentially the same value as the pitch of the Pt templates. For the

600 nm pitch templates, the period of the simulated final-stage film was instead ~1/2 the template spacing, i.e. in accord with the spacing of the 300 nm pitch Pt template.

The 200 nm templates yielded simulated lamellae with a nominal period of 200 nm and the 600 nm templates resulted in simulated lamellae at 1/2 their nominal spacing. Notably, however, the 400 nm templates did not produce simulated lamellae with a period of 200 nm. This observation suggests that the generation of periods substantially smaller than the natural lamellar period at a given set of illumination conditions may require perfect registry of templates at the desired period, to optically confine pattern formation to those metastable modes.

Figure 9a shows a simulated phototropically grown Se-Te film deposited on a templated Pt substrate having Pt ridges at a pitch of 1.5 μm. A 2DFT spectrum of the image in Figure 9a is provided in Figure 9b. Substantial straightening was observed in the simulated features on and immediately adjacent to the Pt ridges. However, the pattern showed little, if any, straightening of the simulated lamellae in the region between the ridges. The nearest neighbors to the templated ridges exhibited the most straightening, as was also evident in the simulated films in Figure 6. When the spacing of the templated ridges was greater than 2x the lamellar period, substantial pattern defects were observed in localized regions that were farther than 1-2x the lamellar period away from each templated ridge.

Figure 10 shows selected simulated phototropically grown Se-Te films deposited on templated substrates from Figure 6-7 (Figure 10a-e) and their respective absorption profiles (Figure 10f-j). In the simulated film in which templated ridges were spaced at the expected pattern period (Figure 10a, 242 nm), the resulting absorption profile (Figure 10f) demonstrated higher absorption peak intensities in the tips of simulated lamellae than in any other case. In the cases where the pattern period was confined to a value other than 242 nm and where pattern fidelity

remained high (i.e. Figure 10b-c, 200 nm and 300 nm spaced ridges), the absorption profiles (Figure 10g-h) showed a response comparable to that in Figure 10f, albeit with slightly lower absorption peak intensities in the tips of the lamellae. Furthermore, when the templated ridge spacing was very far out of resonance with the natural lamellar period, as in Figure 10d (400 nm spaced ridges), the obseved lower pattern fidelity and associated interstitial defects were concomitant with a decreased absorption in both the tips and entire volume of the simulated lamellae (Figure 10i). Even though the primary pattern period observed in Figure 10d was 400 nm, the "double-hump" hotspot peaks observed in the absorption profile in Figure 10i illustrate the competition between pattern confinement via the templated ridges and the optically directed natural lamellar period. When the templated ridge spacing was in resonance with the natural lamellar period but at a distance equivalent to 3x the period (Figure 10e, 726 nm spaced ridges), the absorption profile (Figure 10j) demonstrated a mixed response. Some areas had absorption peak intensities comparable to Figure 10f-h, and other areas had lower absorption peak intensities due to the less regular and more inhomogeneous morphology in those cases.

DISCUSSION

1. Physical Mechanism of Development of Order in Phototropically Grown Se-Te Films by Patterning of Optical Scatterers

The inorganic phototropic growth process entails the optically directed spontaneous development of anisotropic, ordered structures from an initially isotropic substrate and isotropic solution with no chemical directing agents. Phototropic growth can be performed under mild conditions, i.e., at room temperature, on any conductive substrate, and under low illumination

intensity (as low as a few mW-cm^{-2}), with no requirement for source coherency. Furthermore, as an optically driven process yielding primarily amorphous material, neither the crystallite orientation of the Se-Te alloy nor the unique structural characteristics of Se or Te helical chains contribute substantially to the resulting morphology of phototropically grown films.[1, 6] Due to dark deposition processes, a portion of the mass of the photoelectrodeposited film, primarily and especially during the initial nucleation process, is deposited randomly. The interaction of a subset of these randomly distributed scatterers with the incident illumination produces a near-field interference pattern that stimulates further localized mass deposition and film growth, which in turn produces localized hot spots for light absorption that further focus the subsequent mass deposition and film growth. This concept is demonstrated in Scheme 1a-b, in which an initially random distribution of nucleates produces optical scattering intensity that reinforces morphological expression during the phototropic growth process. This feedback-driven emergent light-matter interaction in inorganic phototropic materials results in the characteristic lamellar morphology of phototropically grown films that are deposited under polarized illumination. Optical scatterers can be introduced before any deposition occurs by physically templating the growth substrate with patterned scatterers (Figure 2). Inorganic phototropic growth of Se-Te on these templated substrates results in precise morphological control and produced pattern fidelities and pattern periods that are otherwise inaccessible by growing films under the same conditions on non-templated substrates (Figure 3-5). The role of templated ridges as optical scatterers is illustrated in Scheme 1c-f. In the trivial case where optical scatterers are in mutual optical resonance (Scheme 1c-d), the period of scattered intensity maxima equals the expected lamellar period ($\lambda/2n$). In contrast, when the optical scatterers are out of precise resonance (Scheme 1e-f),

the period of scattered intensity maxima is substantially different from the $\lambda/2n$ value, which ultimately results in lamellae with an equivalent pattern period (equal to the template spacing).

Increases in the randomness of the initial nucleation step (with accompanying smaller inter-nucleate spacings) result in phototropically grown films that have increased fidelity in their patterns, as well as the development of an oriented lamellar morphology at earlier stages of the deposition process.[6] This behavior is consistent with the physical explanation that an initial distribution of mass with smaller and more random inter-nucleate spacings contains a larger subset of optical scatterer-pairs that have a spacing suitable to mutually reinforce growth and thus result in the formation of ordered, oriented lamellae. Specifically, for an arbitrary set of illumination conditions (i.e., wavelength and polarization), smaller nucleate spacings should result in more constructive interference between the required subsets of nucleates and thus promote growth at a given wavelength and polarization. This behavior is in accord with experimental observations of lamellae with a pattern period and orientation that is responsive to the characteristics of the optical excitation in essentially an arbitrary direction and arbitrary wavelength above the band gap of the depositing material.

In this work, we further explored the consistency of the experimentally observed film growth characteristics with expectations based on this mechanism, by pre-positioning the optical scatterers through the lithographic patterning of ridges spaced at a precise distance from one another. The resulting, near-perfect pattern fidelity, and excellent agreement between the highly defined observed pattern periods and the underlying ridge spacing, collectively support the hypothesis that the initial distribution of optical scatterers plays a predominant role in both the morphological expression and pattern fidelity of the resulting phototropically grown films. Moreover, the long-range disorder and short-range undulations in the photoelectrodeposited Se-

Te films are not intrinsic to the inorganic phototropic growth process, but consistently can be assigned as a result of the distribution in distances between initially deposited scatterers in the random distribution of nucleates produced by the initial film growth phase on unpatterned substrates.

2. Probing the Interaction Length of Inorganic Phototropic Emergent Film Growth Effects by Patterning Optical Scatterers

The results in Figure 3-6 demonstrate that increasing the spacing of the templated ridges (relative to the number of lamellae between adjacent ridges) resulted in a smaller degree of confinement of the pattern period as well as a decrease in the fidelity of the resulting pattern. In both simulation and experiment, the pattern fidelity of the templated phototropically grown films decreased sharply when templated optical scatterers were spaced apart by a distance greater than 2x the period of the lamellar pattern that resulted from phototropic growth on the corresponding templated substrates.

The results in Figure 7-8 demonstrate that the pattern periods of phototropically grown films on templated substrates are primarily a function of the spacing between the template ridges, rather than the illumination wavelength, as would be the case for phototropic growth on non-template substrates. However, as shown in Figure 9, phototropically grown films deposited on templated substrates with a relatively large spacing relative to the natural lamellar period (1.5 μm, or > 6x the expected pattern period at the given growth conditions) demonstrated little, if any, improvement in fidelity or order, and no clear morphological control of the individual lamellae at a distance more than 1-2x the average pattern period away from the templated ridges. This behavior was further demonstrated by the absorption profiles for simulated phototropically grown Se-Te films in Figure 10f-j. The point at which the strongly optically confining behavior of templated

ridges starts to break down can be understood as a result of either: templated ridges being too far out of resonance with the natural lamellar period (as was the case in Figure 10d and i, with 400 nm spaced ridges) and/or templated ridges being in resonance with the natural lamellar period but with an inter-ridge spacing of more than 2x the resulting lamellar period (Figure 10e and j, with 726 nm spaced ridges).

Specifically, during inorganic phototropic growth, a pair of any two dipole scatterers in mutual near-field optical communication will contribute substantially to the local morphological expression of lamellae by focusing the near-field light intensity to hot spots near these scatterers. Conversely, the development of the lamellar morphology will be substantially diminished in a growing film that does not contain (or produce through deposition) optical scatterers with an appropriate minimum spacing. Major consequences of this phenomenon are observed in the fidelity of phototropically grown films as shown herein. Though phototropic growth is a demonstrably near-field phenomenon, the long-range order and alignment of near-field optical scatterer-pairs in or out of mutual resonance with one another is likely a major source of the pattern fidelity in resulting phototropically grown films. The implications of the relatively short-range influence of scattering processes in inorganic phototropic growth is that the template must be ordered on a length scale commensurate with a lamellar feature length, as opposed to a length scale commensurate with 10 or 100 lamellar features, to impose fidelity, alignment, and order in the resulting photoelectrodeposit, at least for the phototropic materials and growth processes explored to date.

CONCLUSIONS

Extrinsic optical scatterers can act as structure and morphology-directing templates for the inorganic phototropic growth of Se-Te films. Extrinsic scatterers can produce pattern periods and pattern fidelities that are not normally accessible by film growth on non-templated substrates. Templated substrates can moreover confine the pattern period in phototropically grown Se-Te films. Templates act simultaneously as oriented nucleation sites and as oriented scattering sites, leading to high fidelity structures in phototropically grown films, and additionally serve to expand the range of pattern periods accessible to phototropically grown films under a given set of illumination conditions. Optical simulations confirmed the ability of templated patterned scatterers to confine pattern periods in phototropically grown films. For example, phototropically grown Se-Te films on templated substrates can have periods at least ~80-160% of the natural period for film growth under a given set of illumination conditions. Hence, the use of optical scatterers as templates during phototropic growth allows for high pattern fidelity and for morphological modes that are otherwise inaccessible through the phototropic growth process. The templated optical scatterers have also allowed elaboration of the mechanism of oriented and ordered films by inorganic phototropic growth, as well as the length-scale of the light-matter interaction that controls and induces fidelity and order as an emergent property in phototropically growing inorganic films.

SUPPORTING INFORMATION.

Discussion of pattern fidelity and peak-fitting procedures in 2D FT spectra, additional simulations.

AUTHOR INFORMATION.

Corresponding Author
*Email: nslewis@caltech.edu.

Notes
The authors declare no competing financial interest.

ACKNOWLEDGEMENTS.

This work was supported by the National Science Foundation under Award Number DMR1905963.

REFERENCES

1. Sadtler, B.; Burgos, S. P.; Batara, N. A.; Beardslee, J. A.; Atwater, H. A.; Lewis, N. S., Phototropic growth control of nanoscale pattern formation in photoelectrodeposited Se-Te films. *Proc Natl Acad Sci U S A* **2013,** *110* (49), 19707-12.
2. Carim, A. I.; Batara, N. A.; Premkumar, A.; Atwater, H. A.; Lewis, N. S., Self-Optimizing Photoelectrochemical Growth of Nanopatterned Se–Te Films in Response to the Spectral Distribution of Incident Illumination. *Nano Lett* **2015,** *15* (10), 7071-7076.
3. Carim, A. I.; Batara, N. A.; Premkumar, A.; Atwater, H. A.; Lewis, N. S., Polarization Control of Morphological Pattern Orientation During Light-Mediated Synthesis of Nanostructured Se-Te Films. *ACS Nano* **2016,** *10* (1), 102-11.
4. Carim, A. I.; Batara, N. A.; Premkumar, A.; May, R.; Atwater, H. A.; Lewis, N. S., Morphological Expression of the Coherence and Relative Phase of Optical Inputs to the Photoelectrodeposition of Nanopatterned Se-Te Films. *Nano Lett.* **2016,** *16* (5), 2963-2968.
5. Simonoff, E.; Lichterman, M. F.; Papadantonakis, K. M.; Lewis, N. S., Influence of Substrates on the Long-Range Order of Photoelectrodeposited Se-Te Nanostructures. *Nano Lett* **2019,** *19* (2), 1295-1300.
6. Simonoff, E.; Van Munoz, L. X.; Lewis, N. S., Increased spatial randomness and disorder of nucleates in dark-phase electrodeposition lead to increased spatial order and pattern fidelity in phototropically grown Se-Te electrodeposits. *Nanoscale* **2020,** *12* (44), 22478-22486.
7. Carim, A. I.; Hamann, K. R.; Batara, N. A.; Thompson, J. R.; Atwater, H. A.; Lewis, N. S., Template-free synthesis of periodic three-dimensional PbSe nanostructures via photoelectrodeposition. *J Am Chem Soc* **2018,** *140* (21), 6536-6539.
8. Hamann, K. R.; Carim, A. I.; Meier, M. C.; Thompson, J. R.; Batara, N. A.; Yermolenko, I. S.; Atwater, H. A.; Lewis, N. S., Optically tunable mesoscale CdSe morphologies via inorganic phototropic growth. *Journal of Materials Chemistry C* **2020,** *8* (36), 12412-12417.
9. Hulteen, J. C.; Van Duyne, R. P., Nanosphere lithography: A materials general fabrication process for periodic particle array surfaces. *Journal of Vacuum Science & Technology A: Vacuum, Surfaces, and Films* **1995,** *13* (3), 1553-1558.
10. Sun, F.; Cai, W. P.; Li, Y.; Cao, B.; Lu, F.; Duan, G.; Zhang, L., Morphology Control and Transferability of Ordered Through-Pore Arrays Based on the Electrodeposition of a Colloidal Monolayer. *Advanced Materials* **2004,** *16* (13), 1116-1121.
11. Xia, Y.; Whitesides, G. M., Soft Lithography. *Angewandte Chemie International Edition* **1998,** *37* (5), 550-575.
12. Soolaman, D. M.; Yu, H.-Z., Monolayer-Directed Electrodeposition of Oxide Thin Films: Surface Morphology versus Chemical Modification. *The Journal of Physical Chemistry C* **2007,** *111* (38), 14157-14164.
13. Ogata, Y.; Kobayashi, K.; Motoyama, M., Electrochemical metal deposition on silicon. *Curr Opin Solid St M* **2006,** *10* (3-4), 163-172.
14. Ingole, S.; Aella, P.; Hearne, S. J.; Picraux, S. T., Directed assembly of nanowire contacts using electrodeposition. *Applied Physics Letters* **2007,** *91* (3), 033106.
15. Chen, P.; Zhang, R.; Zhao, Z. M.; Xi, D. J.; Shen, B.; Chen, Z. Z.; Zhou, Y. G.; Xie, S. Y.; Lu, W. F.; Zheng, Y. D., Growth of high quality GaN layers with AlN buffer on Si(111) substrates. *Journal of Crystal Growth* **2001,** *225* (2-4), 150-154.

16. Chang, J. R.; Yang, T. H.; Ku, J. T.; Shen, S. G.; Chen, Y. C.; Wong, Y. Y.; Chang, C. Y., GaN Growth on Si(111) Using Simultaneous AlN/α-Si_3N_4Buffer Structure. *Japanese Journal of Applied Physics* **2008,** *47* (7), 5572-5575.
17. Kim, J. H.; Lange, F. F., Seeded Epitaxial Growth of $PbTiO_3$ Thin Films on (001) $LaAlO_3$ using the Chemical Solution Deposition Method. *Journal of Materials Research* **2011,** *14* (4), 1626-1633.
18. Gu, C. Z., Enhanced electron emission from diamond film deposited on pre-seeded Si substrate with nanosized diamond power. *Applied Surface Science* **2005,** *251* (1-4), 225-229.
19. Zhu, D.; Ming, L.; Huang, M.; Zhang, Z.; Huang, X., Seed-assisted growth of high-quality multi-crystalline silicon in directional solidification. *Journal of Crystal Growth* **2014,** *386*, 52-56.
20. Tamboli, A. C.; Chen, C. T.; Warren, E. L.; Turner-Evans, D. B.; Kelzenberg, M. D.; Lewis, N. S.; Atwater, H. A., Wafer-Scale Growth of Silicon Microwire Arrays for Photovoltaics and Solar Fuel Generation. *IEEE Journal of Photovoltaics* **2012,** *2* (3), 294-297.
21. Yue, L.; Gao, W.; Zhang, D.; Guo, X.; Ding, W.; Chen, Y., Colloids seeded deposition: growth of titania nanotubes in solution. *J Am Chem Soc* **2006,** *128* (34), 11042-3.
22. Sugunan, A.; Warad, H. C.; Boman, M.; Dutta, J., Zinc oxide nanowires in chemical bath on seeded substrates: Role of hexamine. *Journal of Sol-Gel Science and Technology* **2006,** *39* (1), 49-56.
23. Baruah, S.; Dutta, J., Hydrothermal growth of ZnO nanostructures. *Sci Technol Adv Mater* **2009,** *10* (1), 013001.
24. Chen, H.-G.; Li, Z.-W.; Lian, H.-D., Control of epitaxial growth orientation in ZnO nanorods on c-plane sapphire substrates. *Thin Solid Films* **2010,** *518* (19), 5520-5524.
25. Graham, L. M.; Cho, S.; Kim, S. K.; Noked, M.; Lee, S. B., Role of boric acid in nickel nanotube electrodeposition: a surface-directed growth mechanism. *Chem Commun (Camb)* **2014,** *50* (5), 527-9.
26. Choi, K. S., Shape control of inorganic materials via electrodeposition. *Dalton Trans* **2008,** (40), 5432-8.
27. Mettela, G.; Kulkarni, G. U., Facet selective etching of Au microcrystallites. *Nano Research* **2015,** *8* (9), 2925-2934.
28. Boercker, J. E.; Schmidt, J. B.; Aydil, E. S., Transport Limited Growth of Zinc Oxide Nanowires. *Crystal Growth & Design* **2009,** *9* (6), 2783-2789.
29. Li, H. F.; Kar, A. K.; Parker, T.; Wang, G. C.; Lu, T. M., The morphology and texture of Cu nanorod films grown by controlling the directional flux in physical vapor deposition. *Nanotechnology* **2008,** *19* (33), 335708.
30. Baruah, S.; Dutta, J., pH-dependent growth of zinc oxide nanorods. *Journal of Crystal Growth* **2009,** *311* (8), 2549-2554.
31. Lymperakis, L.; Neugebauer, J., Large anisotropic adatom kinetics on nonpolar GaN surfaces: Consequences for surface morphologies and nanowire growth. *Physical Review B* **2009,** *79* (24).
32. Krauskopf, A. A.; Jimenez, A. M.; Lewis, E. A.; Vogt, B. D.; Muller, A. J.; Kumar, S. K., Mechanisms of Directional Polymer Crystallization. *ACS Macro Lett* **2020,** *9* (7), 1007-1012.
33. Dasog, M.; Carim, A. I.; Yalamanchili, S.; Atwater, H. A.; Lewis, N. S., Profiling Photoinduced Carrier Generation in Semiconductor Microwire Arrays via Photoelectrochemical Metal Deposition. *Nano Lett.* **2016,** *16* (8), 5015-5021.

34. Qin, C.; Campbell, B. M.; Shen, M.; Zhao, T.; Sadtler, B., Light-Driven, Facet-Selective Transformation of Cuprous Oxide Microcrystals to Hollow Copper Nanoshells. *Chemistry of Materials* **2019,** *31* (19), 8000-8011.
35. Yoo, B.; Xiao, F.; Bozhilov, K. N.; Herman, J.; Ryan, M. A.; Myung, N. V., Electrodeposition of Thermoelectric Superlattice Nanowires. *Advanced Materials* **2007,** *19* (2), 296-299.
36. Hale, G. M.; Querry, M. R., Optical Constants of Water in the 200-nm to 200-µm Wavelength Region. *Appl. Opt.* **1973,** *12*, 555-563.

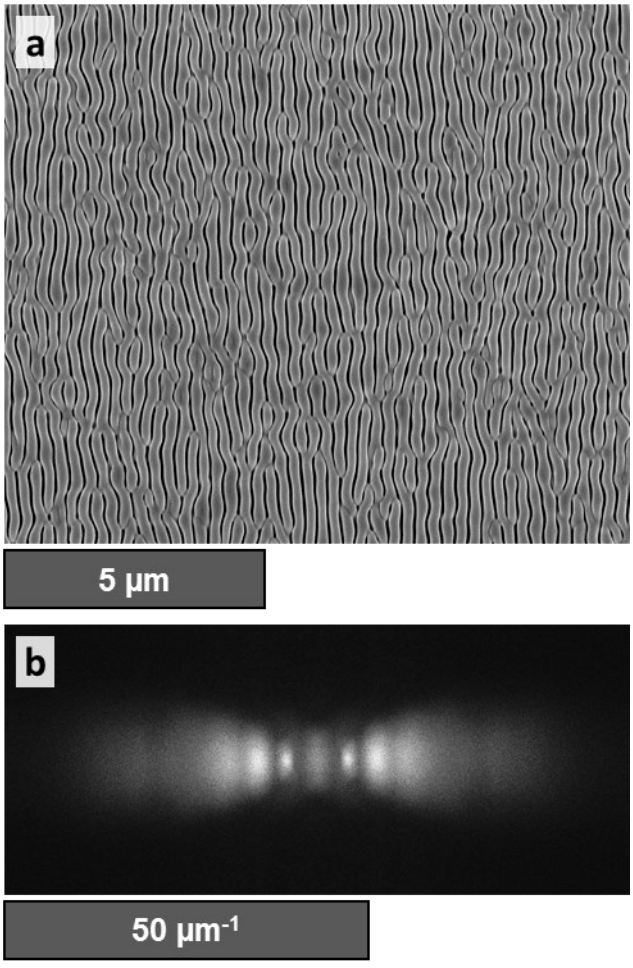

Figure 1. (a) Representative SEM image of a phototropically grown Se-Te film deposited on a Pt-coated n^+-Si substrate with a Ti interlayer. The film was grown under polarized 630 nm excitation from a narrow-band LED. (b) 2D FT spectrum generated from a large-area SEM image of the film in (a).

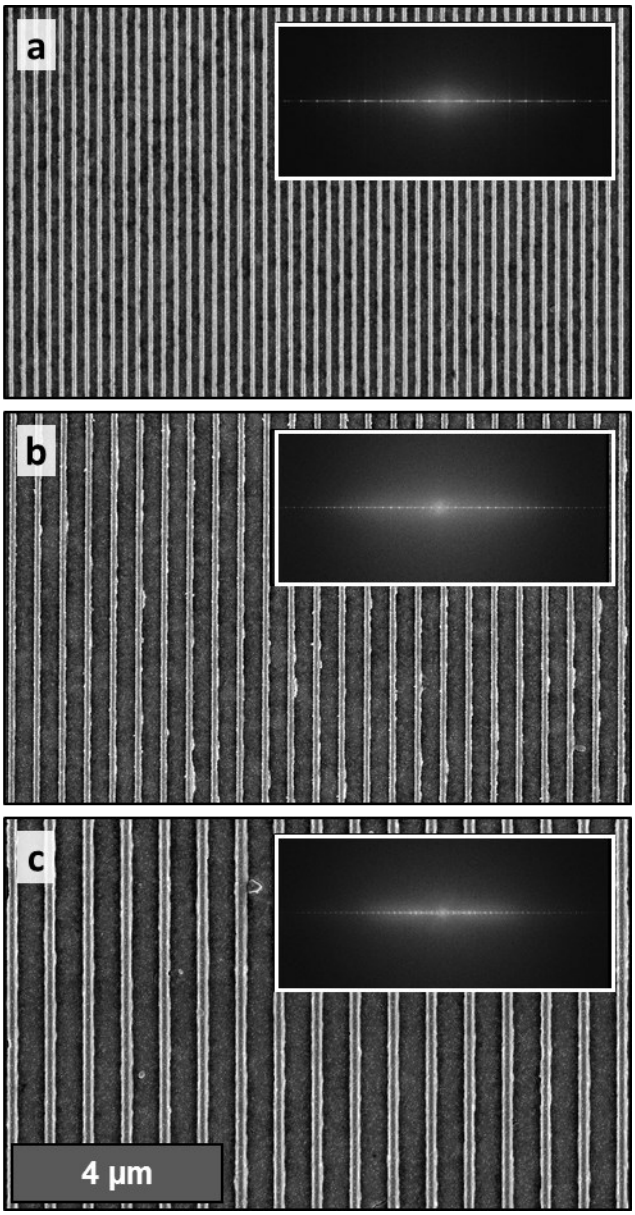

Figure 2. SEM images of templated substrates with ~100 nm wide Pt ridges spaced at a pitch of (a) 242 nm, (b) 484 nm, or (c) 726 nm. Inset images correspond to 2D FT of large-area images of substrates in (a), (b), and (c), respectively. The inset width is 85 μm^{-1}.

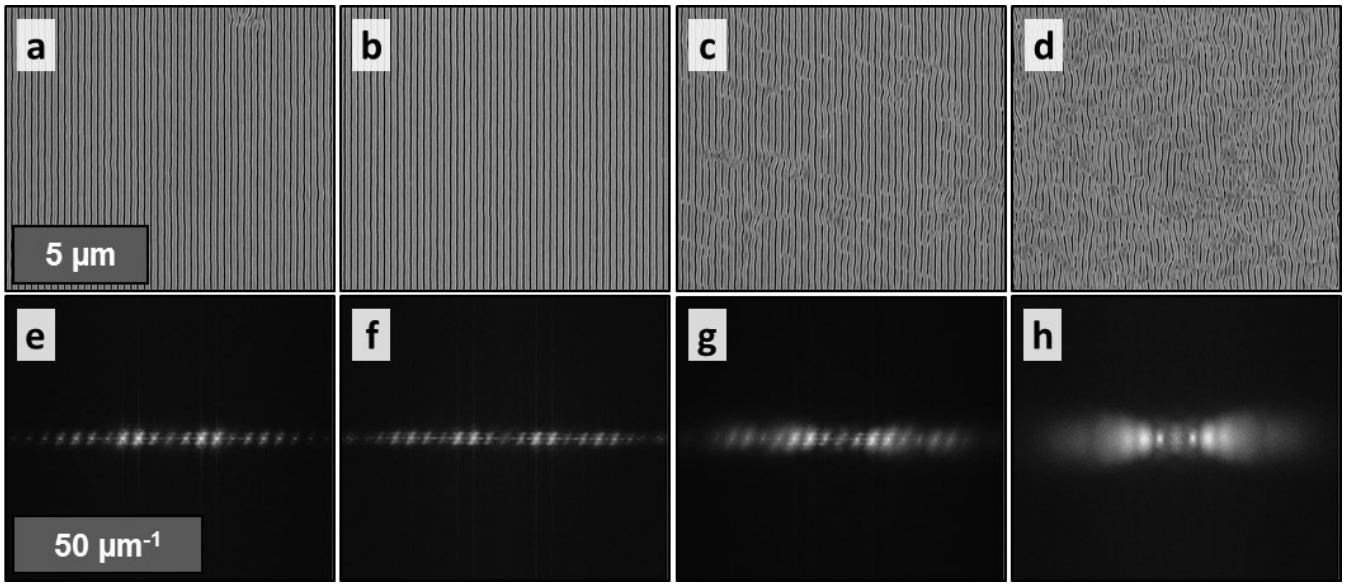

Figure 3. Representative SEM images of phototropically grown Se-Te films deposited on templated substrates having a Pt ridge pitch of (a) 242 nm, (b) 484 nm, or (c) 726 nm. The films were grown under polarized 630 nm excitation from a narrow-band LED. The Se-Te film in (d) was deposited on a Pt film that was not spatially templated. 2D FT spectra in (e)-(h) generated from large-area SEM images of the films in (a)-(d), respectively.

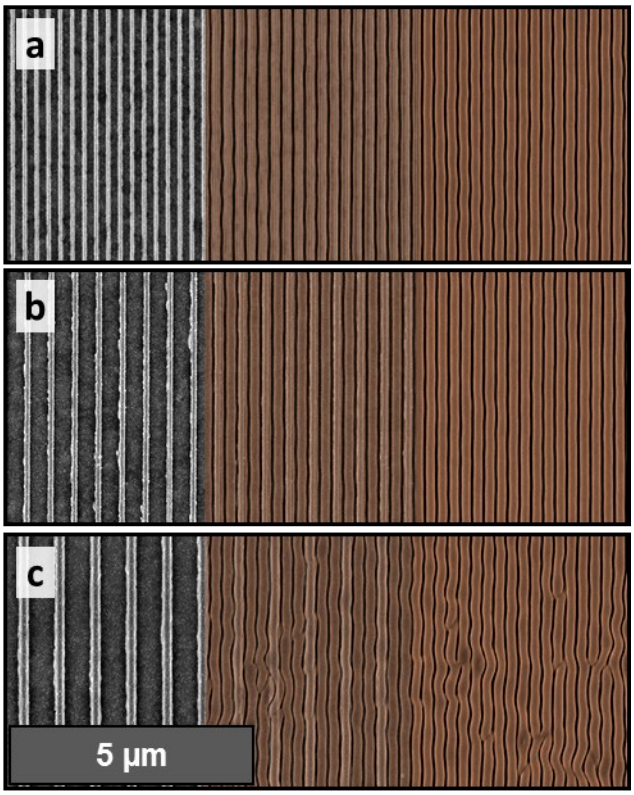

Figure 4. SEM images of templated substrates (left panels) and resulting templated phototropic growth (in orange, right panels). Center panels are overlaid portions of the left and right panels, demonstrating the effect and spacing of the underlying templates. The pitch of Pt ridges on the templated substrates was (a) 242 nm, (b) 484 nm, or (c) 726 nm. All of the films were grown under polarized 630 nm excitation from a narrow-band LED.

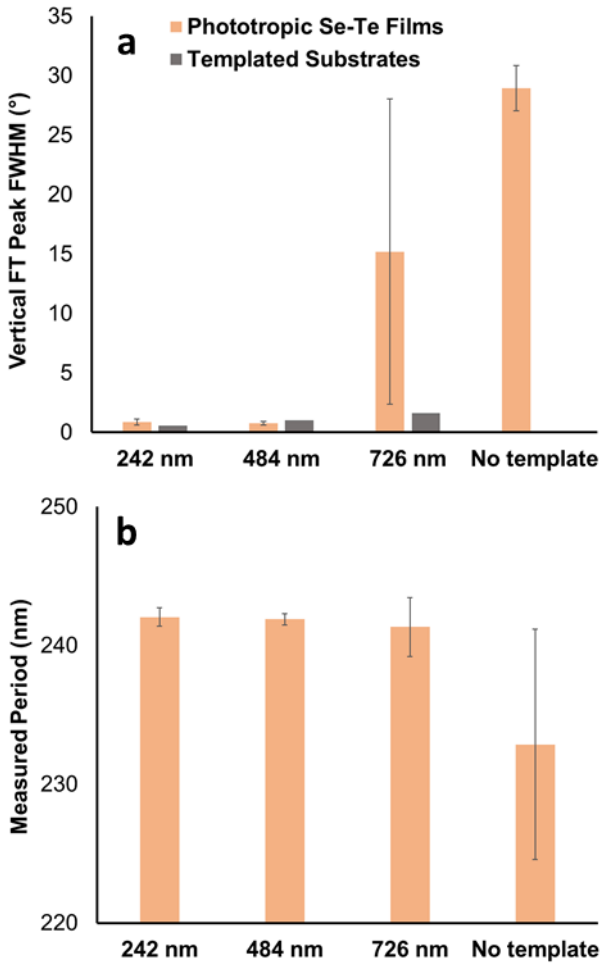

Figure 5. Charts showing (a) pattern fidelity and (b) measured period of templated and non-templated phototropically grown Se-Te films. Pattern fidelity in (a) is calculated as the angular FWHM of the primary peak in the 2D FT spectra generated from large-area images of the respective films. Pattern period in (b) is calculated from the primary peak position in the respective 2D FT spectra.

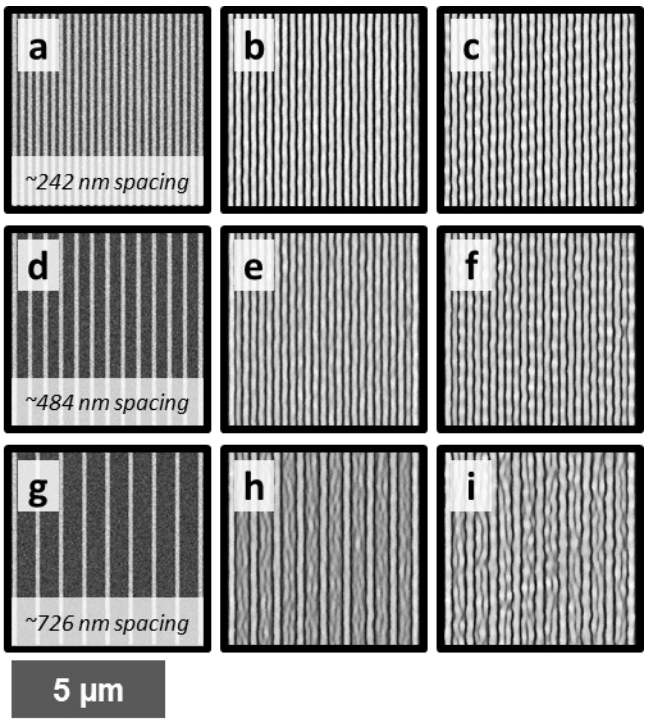

Figure 6. Simulated phototropic growth on templated and substrates with vertically polarized illumination with λ = 630 nm. Simulations were performed with periodic boundary conditions. Substrates have templates with (a)-(c) ~242 nm spacing, (d)-(f) ~484 nm spacing, or (g)-(i) ~727 nm spacing. Panels show (a), (d), (g), initial nucleation step; (b), (e), (h), intermediate stage of growth; and (c), (f), (i), final stage of growth.

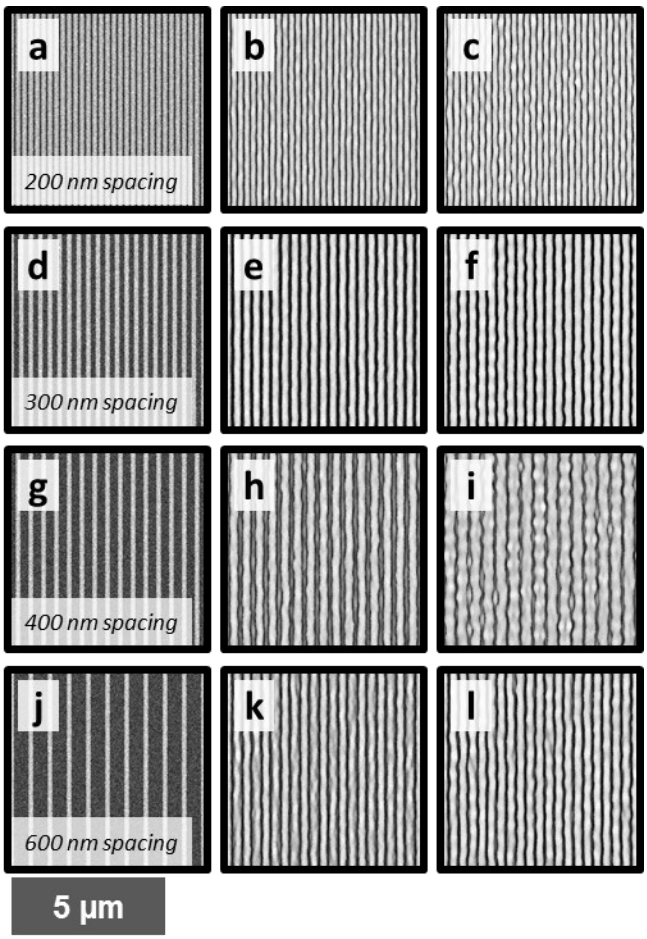

Figure 7. Simulated phototropic growth on templated Pt substrates with vertically polarized illumination with λ = 630 nm. Simulations were performed with periodic boundary conditions. Substrates had 50 nm tall x 100 nm wide Pt ridges with (a)-(c) 200 nm spacing, (d)-(f) 300 nm spacing, (g)-(i) 400 nm spacing, or (j)-(l) 600 nm spacing. Panels show (a), (d), (g), (j) initial nucleation step; (b), (e), (h), (k) intermediate stage of growth; and (c), (f), (i), (l) final stage of growth.

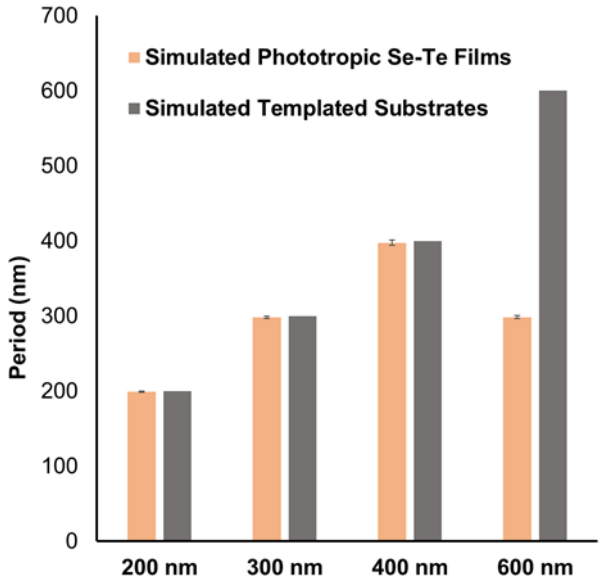

Figure 8. Chart showing the periods of simulated templates and phototropically grown structures in Figure 7. Measured periods for the simulated phototropically grown films were 199 ± 1, 299 ± 2, 398 ± 3, and 299 ± 2 nm for the 200, 300, 400, and 600 nm templated substrates, respectively.

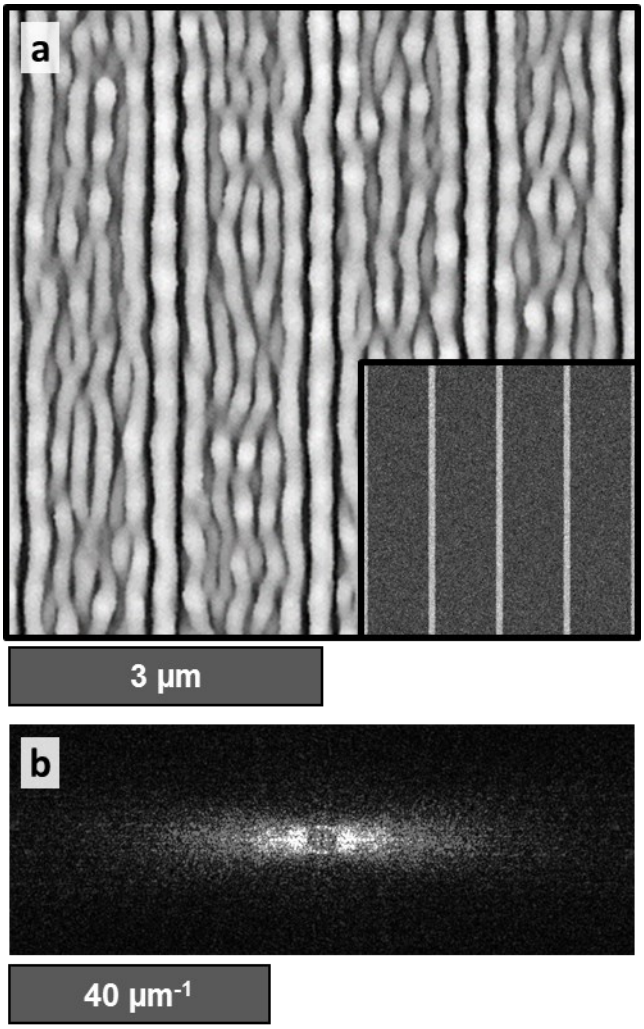

Figure 9. (a) Simulated phototropic growth on a templated substrate with vertically polarized illumination with λ = 630 nm. Simulations were performed with periodic boundary conditions. Substrate has 50 nm tall x 100 nm wide Pt ridges with 1.5 µm spacing. Inset in (a) shows simulated substrate; inset side is 6 µm. (b) 2D FT of image in (a).

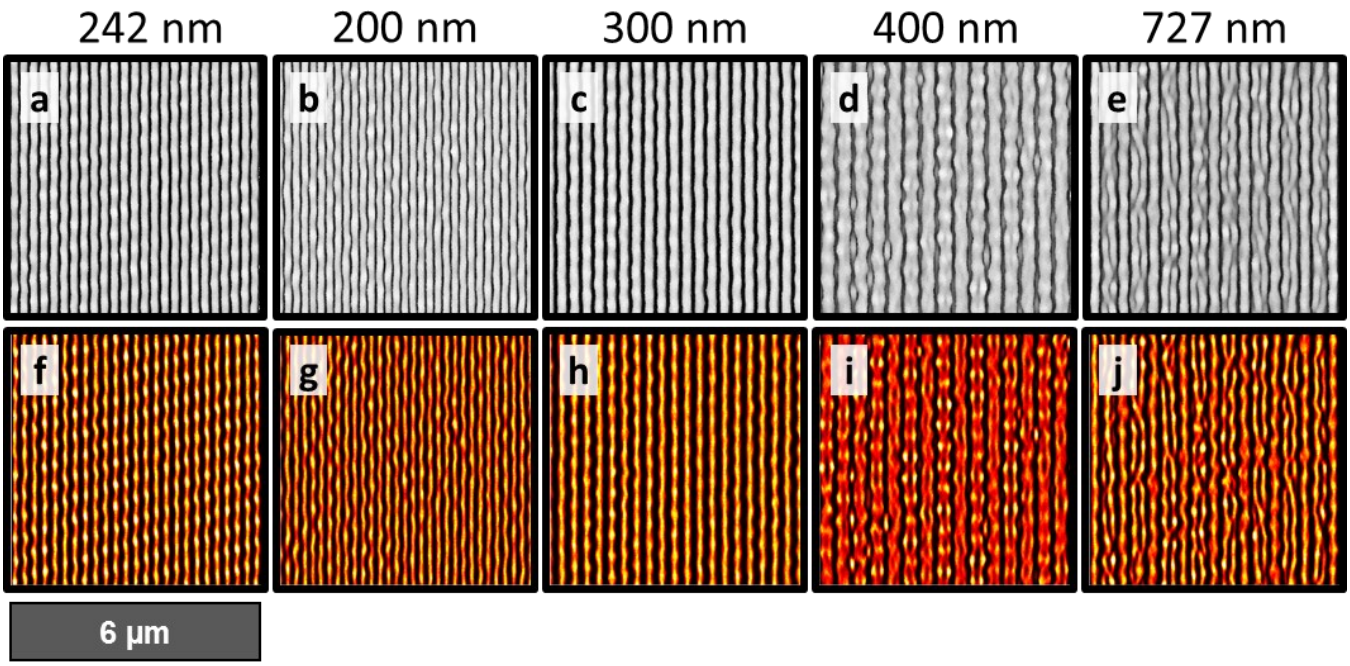

Figure 10. Simulated phototropic growth on templated Pt substrates with vertically polarized illumination with λ = 630 nm. Simulations were performed with periodic boundary conditions. Substrates had 50 nm tall x 100 nm wide Pt ridges with an inter-ridge spacing of (a) 242 nm, (b) 200 nm, (c) 300 nm, (d) 400 nm, and (e) 727 nm. Images in (f)-(j) show light absorption profiles for the simulated films in (a)-(e), respectively.

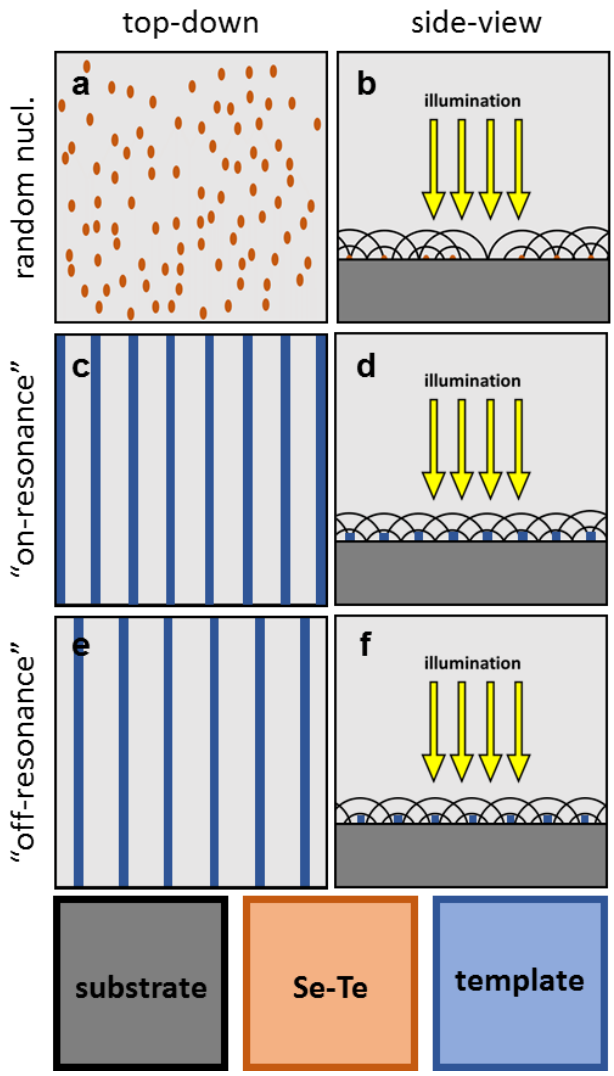

Scheme 1. Schemes showing the interaction of scattered light waves with optical dipole scatterers that are either (a), (b) randomly nucleated Se-Te particles or (c) – (f) lithographically patterned templated ridges. In (c), (d), ridges are spaced such that scattered wave intensity is maximized at each ridge, i.e., ridges are in mutual optical resonance with each other. In (e), (f), ridges are spaced out of optical resonance with each other.

TABLE OF CONTENTS (TOC) GRAPHIC